DDMSA-U-Net: A Lightweight Deep Learning Framework for Multi-Spectral Change Detection for Agricultural Land Use Monitoring

Layth Hussein Jasim[1], *P.* Girish[2], *Harshitha* Deepanjali[3], *Sarala*. D V[4*], and *Sahana*. M P[5]

[1]Department of Computers Techniques Engineering, College of Technical Engineering, The Islamic University, Najaf, Iraq
[2]Department of Civil Engineering, Dayananda Sagar Academy of Technology and Management, Bengaluru, India
[3]Department of Information Science and Engineering, Dayananda Sagar Academy of Technology and Management, Bengaluru, India
[4]Department of Computer Science and Engineering, BMS College of Engineering, Bengaluru, India
[5]Department of Computer Science and Engineering, Dayananda Sagar College of Engineering, Bengaluru, India

Abstract. The change detection approach using remote sensing is vital in agriculture monitoring; however, the existing approach lacks efficiency in terms of boundary accuracy and sensitivity to spatial scales, and suffers from background noise. Such constraints make it difficult to map transitions such as crop rotations, fallow, and urban encroachment, particularly in heterogeneous landscapes. This research proposes Depthwise Dilated Multi-Spatial Attention U-Net (DDMSA-U-Net), which is a light architecture that enhances the accuracy of change detection achieved with both Landsat- 8 and Sentinel- 2 satellite images. The model integrates depth-wise separable convolutions, dilated multiscale feature extraction, and multispatial attention mechanisms to enhance spatial discrimination and reduce computational costs. The methodology includes preprocessing of multi-temporal satellite imagery, supervised training, stratified sampling, and post-classification comparisons to assist in change detection. Validation was carried out based on the seasonal crop observations of 2021-2024. Compared to traditional methods, DDMSA-U-Net improved in terms of classification and change detection with an overall accuracy of 91.6-96.6 and Kappa values above 0.85 for all cases. These findings highlight the usefulness of the model for observations of agricultural transitions.

1 Introduction

High-resolution Remote Sensing (RS) imagery is vital for crop monitoring and land-use Change Detection (CD). Capturing dynamic ground changes requires a dense temporal series, whereas fine spatial resolution is essential for depicting surface texture and structure, which is critical for accurate land cover classification and quantitative analysis. [1]. The importance of tracking environmental changes, such as built, marine, and natural environments, cannot be overstated [2]. Therefore, RS is increasingly used to monitor land features because of its ability to capture detailed information over large areas, enable synchronized, multi-resolution observations of the Earth's surface, offer a wide detection range, real-time responsiveness, and independence from ground conditions, making it crucial for monitoring land cover changes across both global and local scales [3][4][5]. RS and Geographic Information System (GIS) tools are widely used to detect, classify, and map land changes using various methods and databases, where human assessment is complex in remote locations [6][7]. Rich, free, and open RS data sources, such as Sentinel, Landsat, and GF series, provide a strong foundation for realizing these applications [8].

In contrast, object-based approaches use spatial and spectral information from high-resolution imagery to segment and classify the land changes. For analyzing heterogeneous landscapes and addressing pixel-based NDVI limitations by incorporating contextual information, this method is more suitable. Nevertheless, they are computationally intensive and require substantial ground-truth data, which are often unavailable in remote regions.[9]. Land use structure is used to describe the spatial proportion and spatial combination relationships of various land-use types [10]. Despite the availability of satellite data and advanced GIS tools, existing CD models often suffer from poor boundary precision, limited multi-scale sensitivity, high computational cost, and weak generalization across sensors, such as Sentinel-2 and Landsat-8. These gaps degrade the accurate mapping of subtle transitions such as crop rotation and fallow cycles. To overcome these challenges, The DDMSA-U-Net model is proposed, which is a lightweight, high-performing architecture integrating Depth-Wise Separable Convolutions (DWSC) , dilated multiscale features, and multispatial attention for enhanced CD accuracy. DWSC, which split standard operations into depth-wise and pointwise steps, considerably reduce the number of parameters and computational load. This

* Corresponding author: saraladv.cse@bmsce.ac.in

enables efficient processing of high-resolution imagery without compromising the feature extraction quality. The contribution of this research is as follows:

- Utilizes multi-temporal Sentinel-2 and Landsat-8 imagery to ensure seasonal and sensor-level consistency in change detection. It produces both binary and "from-to" transition maps, enabling precise tracking of agricultural dynamics with validated high accuracy and agreement scores.
- The dilated Multi-Scale Feature Extraction and Fusion module (DMSFEF) uses Dilated Convolutions with varying rates to extract spatial patterns at multiple scales simultaneously. This expands the receptive field, allowing the model to detect both fine and coarse changes in the land cover.
- DWSC multiscale spatial attention (DMSSA) adaptively emphasizes relevant spatial regions while suppressing background noise across multiple scales. This improves the boundary precision and helps distinguish visually similar land use classes.

The remaining sections of this research is organized as follows. Section 2 presents a literature survey. Section 3 describes the datasets, preprocessing steps, and DDMSA-U-Net model. Section 4 presents the experimental setup and evaluation process. Section 5 presents the results, compares model performance, and discusses the key findings. Section 6 concludes the research and suggests possibilities for future research.

2 Literature review

Recent advancements in RS-based land change detection (CD) are reviewed in this section, highlighting the integration of multisource satellite imagery with Machine Learning (ML) and DL frameworks.

Muchelo et al. [11] presented multi-temporal Landsat imagery with supervised classification to analyze land use and land cover transitions in Kampala, Mbarara, and Uganda. RS detects systematic and random agricultural land changes by comparing spectral signatures across time and constructing transition matrices. The datasets included Landsat scenes from 1989 to 2015 for Kampala and 2002–2016 for Mbarara, supplemented by aerial photographs and field validation. Agricultural land loss was quantified using the gain-to-persistence and swap ratios, revealing that urban expansion systematically targeted fertile zones. A key strength was the distinction between random and systematic transitions, offering nuanced landscape insights. However, the reliance on medium-resolution imagery has limited the detection of fine-scale informal settlements and fragmented patterns.

Wang et al. [12] implemented a deep multimodal temporal semantic segmentation framework (TSSCD) enhanced with ant colony optimization (ACO) to monitor agricultural land conversion in Zhengzhou, China. RS integrated Sentinel-2 and Landsat 7/8 imagery with the China Land Cover Dataset (CLCD), enabling pixel-level tracking of land use transitions over 20 years. The model extracts temporal features using one-dimensional convolutions and corrects inconsistencies via spatiotemporal smoothing filters. Annual composites were generated during the growing season to ensure spectral fidelity and minimize cloud interference. ACO optimized the hyperparameters, improving the robustness in capturing subtle and frequent transitions. A key strength was the joint identification of the timing and type of land cover change, offering fine-grained semantic insights. However, the reliance on band substitution between sensors introduces spectral redundancy, affecting feature discrimination in heterogeneous landscapes.

Zhang et al. [13] employed a random forest classifier to multi-source imagery from Landsat 8, Sentinel-2, and Sentinel-1 to identify immature rubber plantations (IRPs) at early growth stages. RS was conducted using Google Earth Engine with time-series composites at 3-month intervals to capture subtle spectral and structural IRP changes. Twelve scenarios were tested, and combining all the datasets with short intervals yielded the highest accuracy. The dataset spanned plantations from the second to fourth year post-establishment and was validated over Hainan Island, China. The strength was reduced by a typical five-year mapping lag by capturing early phenological signals. However, reliance on frequent cloud-free imagery poses challenges in tropical regions, limiting the temporal consistency in dense canopy zones.

Hosseini et al. [14] implemented a stacked ensemble ML model within the Google Earth Engine to map the cropping intensity in southwest Iran using Sentinel-2 and Landsat-8/9 imagery. RS was conducted by generating monthly composites and applying a heterogeneous ensemble of classifiers: SVM, RF, CART, and GBT, combined through a minimum-distance meta-classifier. Ground-truth samples from 2021 were used for training, and the model was temporally transferred to predict the cropping intensity for other years. The dataset spanned 2019–2023, with 2024 forecasts generated using a cellular automata-Markov model. Strength was generalized across years despite high intra-class variability due to ensemble design and temporal transferability. However, reliance on monthly composites may have limited sensitivity to short-duration cropping cycles, particularly in regions with rapid phenological shifts.

Eisfelder et al. [15Employed supervised random forest classification on Sentinel-1 and Sentinel-2 time-series data from Google Earth Engine to map cropland and crop types across three Ethiopian regions. RS extracted spectral indices and radar backscatter parameters evaluated across 33 model variants to determine the optimal inputs. Field data from 2021 and 2022, covering 18 crop types, served as a reference for training and validation. The final model integrated Sentinel-2 bands, EVI2, NDRe2, Sentinel-1 VV, VH, and Diff metrics to enhance classification robustness. Strength distinguished diverse crop types in smallholder systems using free data and scalable cloud processing. However, limited improvement from radar features suggested reduced Sentinel-1 sensitivity to crop-specific structural variations, especially in mixed-cropping landscapes.

Although recent advancements exist, RS-CD systems face limitations: medium-resolution imagery cannot detect fine-scale features, and spectral redundancy and cloud cover interfere with sensitivity to short crop cycles. Most multimodal models are computationally demanding, and boundary accuracy, multi-scale discrimination, and sensor generalization remain challenging. These gaps are addressed by the proposed DDMSA-U-Net v5 model, which incorporates DWSC, dilated multiscale features, and multispatial attention to improve the CD accuracy on Sentinel-2 and Landsat-8 datasets.

3 Proposed methodology

Figure 1 shows the complete workflow of the proposed DDMSA-U-Net framework for land use change detection. The process begins with multi-temporal satellite image acquisition and preprocessing, followed by sample preparation and model training. The DDMSA-U-Net architecture integrates DWSC, dilated multiscale feature extraction (DMSFE), and spatial attention to enhance segmentation accuracy. A post-classification comparison was used to generate change maps, which were then validated using standard accuracy metrics. The final outputs included classified maps, change maps, and statistical summaries for agricultural monitoring.

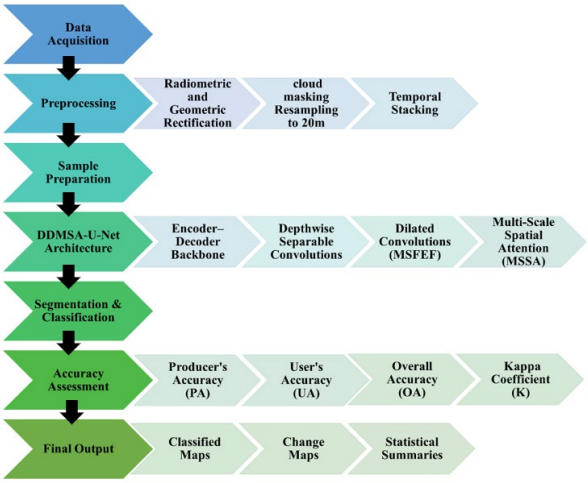

Fig. 1. Workflow of the proposed DDMSA-U-net.

3.1 Dataset and preprocessing

First, the research utilizes multi-temporal satellite imagery from the Sentinel-2 and Landsat-8 missions. These datasets offer complementary spatial, spectral, and temporal characteristics that are suitable for agricultural land-use monitoring.

3.1.1 Dataset description

Sentinel-2 [16] is a European Earth observation mission under the Copernicus program. It provides systematic, free access to high-resolution multispectral imagery across 13 spectral bands: four at 10 m, six at 20 m, and three at 60 m spatial resolution. Twin satellites S-2B and S-2C operate in a phased orbit with a revisit frequency of five days at the equator, supported by S-2A at an offset position. A swath width of 290 km enabled the efficient coverage of large agricultural regions. Sentinel-2 supports applications in vegetation monitoring, land use, and crop assessments.

Landsat-8 [17], launched by NASA and USGS, carries an Operational Land Imager (OLI) and Thermal Infrared Sensor (TIRS). OLI captures visible, NIR, and SWIR bands at 30 m multispectral and 15 m panchromatic resolutions, including new bands for coastal and cirrus detection. TIRS provides thermal imaging at a resolution of 100 m and is co-registered with OLI to produce radiometrically and geometrically corrected 12-bit products. Landsat-8 ensures seasonal global coverage and continuity with previous Landsat missions.

3.1.2 Preprocessing

Sentinel-2 and Landsat-8 images were selected based on their cloud-free conditions and seasonal relevance. Radiometric correction ensures spectral consistency, whereas geometric rectification aligns the imagery for pixel-wise comparisons.

The images were stacked into a temporal data cube, enabling the construction of bi-temporal pairs for the CD. This structure supports the extraction of spectral indices and texture features, which enhances model input quality. preprocessing ensures that the satellite data are clean, spatially aligned, and temporally consistent, forming a reliable foundation for agricultural change analysis.

3.2 Proposed architecture

A DL block, a Depthwise Dilated Multi-Spatial Attention (DDMSA) block, is introduced. The resulting model, referred to as DDMSA-U-Net in Figure 2, is designed to improve the ability to capture multi-scale features and fine spatial structures through multi-scale feature extraction and attention mechanisms.

The key innovation of the DDMSA-U-Net is the integration of the DDMSA block, which consists of two main components, as shown in Figure 3. In addition to the attention mechanism, the convolutional layers in the encoder, decoder, and DMSSA modules were implemented using DWSC. This technique decomposes the standard convolution into two operations: depth-wise convolution and pointwise convolution. It reduces the number of parameters and computational cost while maintaining the spatial resolution of the feature maps.

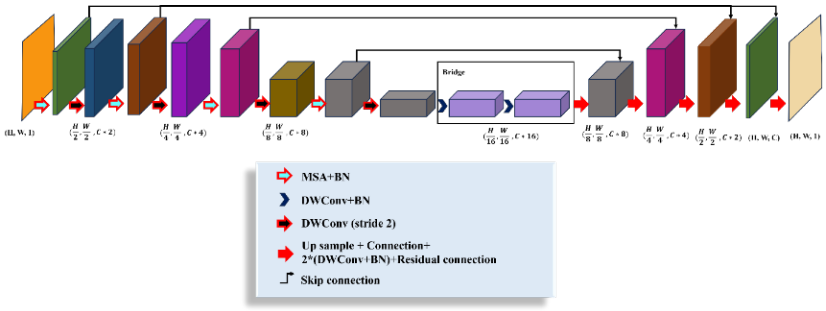

Fig. 2. The architecture of DDMSA-U-Net model.

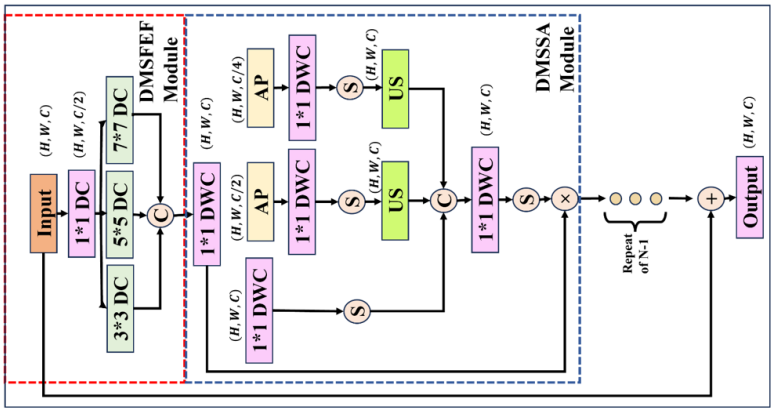

Fig. 3. The architecture of DDMSA block.

The detailed description of each component is as follows:

3.2.1 DMSFE and fusion module (DMSFEF)

The DMSFEF module is designed to extract features at multiple scales. It uses parallel convolutional layers with different receptive fields to capture both the fine and coarse spatial patterns. In DDMSA-U-Net, the DC is used to increase the receptive field without increasing the number of parameters. The outputs from the parallel branches are fused to form a unified feature representation. This fusion enhances the ability of the model to represent complex spatial structures and improves its sensitivity to subtle changes in agricultural land.

3.2.2 DWSC multi-scale spatial attention module (DMSSA)

The DMSSA module was used to generate spatial attention weights across multiple resolutions. Average pooling was applied to produce downsampled versions of the input feature map. These are processed through convolutional layers followed by Leaky ReLU activation, which improves the feature sensitivity and gradient flow. The attention weights were then upsampled and fused to recalibrate the input features. A final sigmoid activation was applied to produce pixel-wise probabilities for CD. This mechanism allows the model to focus on important spatial regions and to improve its ability to detect small and scattered changes.

3.3 Accuracy assessment and CD strategy

The proposed DDMSA-U-Net model was evaluated using standard accuracy metrics. These methods are widely used in RS-based CD tasks and provide a reliable way to measure the performance of both the classification and CD outputs. The accuracy of the classified maps was assessed using the Producer's Accuracy (PA), User's Accuracy (UA), Overall Accuracy (OA), and the Kappa Coefficient (K). Producer's Accuracy indicates how well the model identifies the reference pixels of a given class, whereas the user's accuracy reflects the probability that a pixel classified into a category actually belongs to that category. The overall Accuracy represents the proportion of correctly classified pixels across all classes, and the Kappa Coefficient measures the agreement between the predicted and reference classifications, accounting for chance agreement. To evaluate changes in agricultural land use, the model generates a binary change/no-change map and a detailed "from-to" transition matrix that shows how each land-cover class has changed over time. This method is effective in identifying pixel-level transitions and supports the interpretation of land use dynamics. Validation was performed using stratified sampling,

ensuring that all land-cover classes were adequately represented in the accuracy assessment.

4 Results and discussions

This section presents an inclusive evaluation of the proposed model based on the classification accuracy, change detection, performance analysis, computational efficiency, and statistical validation. The findings justify the robustness of the model over season and dataset, sensitivity to agricultural shift, and its ability to scale large-scale land-use monitoring. The experimental analysis were performed on a high processing computing platform composed of 64-bit Ubuntu Server 20.04 LTS operating system. GeForce RTX 3080 Ti graphics card that had 24GB of video memory supported the intensive data processing needs of the study along with 128GB of host memory. Python 3.10 became the main program language used in the software environment, which relies on the powerful functions of CUDAv11.8 to accelerate the program using a graphic card. This arrangement allowed the maximization of the use of the GPU with computationally intensive work. The model training and evaluations were implemented in the Pytorch 1.11.0 deep learning framework, which has powerful tools and libraries to assist in the creation and testing of complex neural network structures.

4.1 Accuracy assessment of DDMSA-U-Net change map

The Tables 1 and 2 fully evaluate the CD performance of DDMSA-U-Net on Sentinel-2 and Landsat-8 data sources for both land cover and CD. Constant high values of the overall accuracy (up to 98.4) and Kappa coefficients (up to 0.98) validated the reliability of this method for different land cover categories. In terms of Producer and User accuracy, the accuracy of the classification of transitions such as Fallow Land and Wheat is clearly demonstrated. This further clarifies the effectiveness of the CD model in detecting changes in land use and in monitoring and conservation diagnosis.

Table 1. Accuracy metrics for CD change map across multiple land-use transitions from 2021 to 2024 using DDMSA-U-Net model for sentinel-2 dataset.

S.No	Change Class	PA 2021	UA 2021	K 2021	PA 2022	UA 2022	K 2022	PA 2023	UA 2023	K 2023	PA 2024	UA 2024	K 2024
1	Water → Built-up	1.2	0.6	0.5	1.3	0.7	0.6	1.4	0.8	0.6	1.3	0.7	0.6
2	Water → Forest	1.6	0.9	0.7	1.7	1.0	0.8	1.8	1.1	0.8	1.7	1.0	0.8
3	Water → Berseem	1.0	0.5	0.4	1.1	0.6	0.5	1.2	0.6	0.5	1.1	0.6	0.5
4	Water → Wheat	2.5	1.8	1.5	2.6	1.9	1.6	2.7	2.0	1.6	2.6	1.9	1.6
5	Built-up → Water	1.4	0.6	0.4	1.5	0.7	0.5	1.6	0.7	0.5	1.5	0.7	0.5
6	Built-up → Berseem	1.7	0.6	0.9	1.8	0.7	1.0	1.9	0.8	1.0	1.8	0.7	1.0
7	Built-up → Wheat	4.6	4.2	4.0	4.7	4.3	4.1	4.8	4.4	4.2	4.7	4.3	4.1
8	Berseem → Water	0.6	0.7	0.3	0.7	0.8	0.4	0.8	0.9	0.4	0.7	0.8	0.4
9	Berseem → Built-up	12.4	11.5	12.1	12.6	11.7	12.3	12.8	11.9	12.5	12.6	11.7	12.3
10	Berseem → Wheat	3.1	2.7	3.0	3.2	2.8	3.1	3.3	2.9	3.2	3.2	2.8	3.1
11	Berseem→Fallowland	5.4	5.7	5.7	5.6	5.9	5.9	5.8	6.0	6.0	5.6	5.9	5.9
12	Wheat → Water	1.5	1.5	0.1	1.6	1.6	0.2	1.7	1.7	0.2	1.6	1.6	0.2
13	Wheat → Built-up	1.1	1.0	1.3	1.2	1.1	1.4	1.3	1.2	1.5	1.2	1.1	1.4
14	Wheat → Berseem	0.1	0.1	0.1	0.2	0.2	0.2	0.2	0.2	0.2	0.2	0.2	0.2
15	Fallowland→Berseem	6.2	6.0	6.1	6.4	6.2	6.3	6.5	6.3	6.4	6.4	6.2	6.3
16	Fallow land → Wheat	71.5	75.2	74.0	72.8	76.4	75.3	74.1	77.1	76.2	72.8	76.4	75.3
OA Range (%) = 93.7–96.2 and Kappa Range = 0.8569–0.9194													

Table 2. Accuracy metrics for CD change map across multiple land-use transitions from 2021 to 2024 using DDMSA-U-Net model for landsat-8 dataset.

S.No	Change Class	PA 2021	UA 2021	K 2021	PA 2022	UA 2022	K 2022	PA 2023	UA 2023	K 2023	PA 2024	UA 2024	K 2024
1	Water → Built-up	1.0	0.5	0.4	1.1	0.6	0.5	1.2	0.7	0.5	1.1	0.6	0.5
2	Water → Forest	1.4	0.8	0.6	1.5	0.9	0.7	1.6	1.0	0.7	1.5	0.9	0.7
3	Water → Berseem	0.9	0.4	0.3	1.0	0.5	0.4	1.1	0.5	0.4	1.0	0.5	0.4
4	Water → Wheat	2.3	1.6	1.4	2.4	1.7	1.5	2.5	1.8	1.5	2.4	1.7	1.5
5	Built-up → Water	1.2	0.5	0.3	1.3	0.6	0.4	1.4	0.6	0.4	1.3	0.6	0.4
6	Built-up → Berseem	1.5	0.5	0.8	1.6	0.6	0.9	1.7	0.7	0.9	1.6	0.6	0.9
7	Built-up → Wheat	4.3	3.9	3.7	4.4	4.0	3.8	4.5	4.1	3.9	4.4	4.0	3.8
8	Berseem → Water	0.5	0.6	0.2	0.6	0.7	0.3	0.7	0.8	0.3	0.6	0.7	0.3
9	Berseem → Built-up	11.8	10.9	11.4	12.0	11.1	11.6	12.2	11.3	11.7	12.0	11.1	11.6
10	Berseem → Wheat	2.9	2.5	2.8	3.0	2.6	2.9	3.1	2.7	3.0	3.0	2.6	2.9
11	Berseem→Fallowland	5.2	5.5	5.5	5.4	5.7	5.7	5.6	5.8	5.8	5.4	5.7	5.7
12	Wheat → Water	1.3	1.3	0.1	1.4	1.4	0.2	1.5	1.5	0.2	1.4	1.4	0.2
13	Wheat → Built-up	1.0	0.9	1.2	1.1	1.0	1.3	1.2	1.1	1.4	1.1	1.0	1.3
14	Wheat → Berseem	0.1	0.1	0.1	0.2	0.2	0.2	0.2	0.2	0.2	0.2	0.2	0.2
15	Fallowland→Berseem	6.0	5.8	5.9	6.2	6.0	6.1	6.3	6.1	6.2	6.2	6.0	6.1
16	Fallowland → Wheat	70.2	74.0	73.1	71.5	75.1	74.2	72.8	76.0	75.3	71.5	75.1	74.2
OA Range (%) = 91.6–96.6 and Kappa Range = 0.8402–0.9271													

4.2 Performance analysis of segmentation model

In this section, a comparative analysis, as shown in Figure 4, of the segmentation using the Dice Similarity Coefficient (DSC) and Hausdorff Distance (HD95) is presented. The DDMSA-U-Net model shows improved performance compared to the baseline and attention-augmented variants of U-Net on both the datasets, demonstrating better compliance with class boundaries and consistency at the aggregation scale, confirming its effectiveness in delineating agricultural change patterns with minimal error.

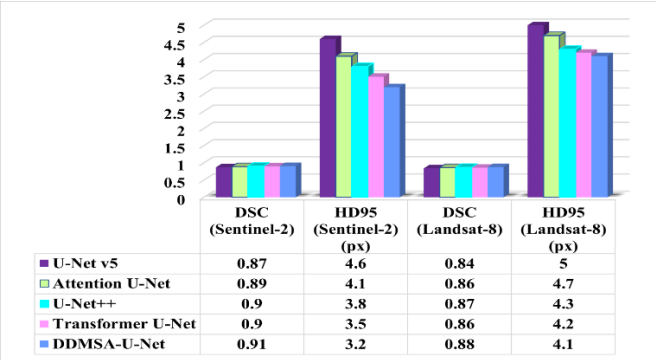

	DSC (Sentinel-2)	HD95 (Sentinel-2) (px)	DSC (Landsat-8)	HD95 (Landsat-8) (px)
U-Net v5	0.87	4.6	0.84	5
Attention U-Net	0.89	4.1	0.86	4.7
U-Net++	0.9	3.8	0.87	4.3
Transformer U-Net	0.9	3.5	0.86	4.2
DDMSA-U-Net	0.91	3.2	0.88	4.1

Fig. 4. The performance comparison of segmentation models.

4.3 Computational complexity

The architectural efficiency of DDMSA-U-Net was compared to competing model architectures considering the number of parameters, FLOPs, and inference time, as shown in Table 3. Even after the enhanced representational capacity, DDMSA-U-Net maintained a better computational footprint, achieving faster inference and lower memory overhead. This balance of accuracy and efficiency makes it suitable for large-scale, real-time land-use monitoring. Table 4 shows computational complexity analysis of segmentation models on sentinel-2 dataset.

Table 3. Computational complexity analysis of segmentation models on sentinel-2 dataset.

Sentinel-2			
Model Variant	**Parameters (Millions)**	**FLOPs (GigaOps)**	**Inference Time (ms/image)**
U-Net v5	31.2	45.6	120
Attention U-Net	34.5	48.3	135
U-Net++	38.1	52.7	150
DDMSA-U-Net v5	29.7	41.3	110

Table 4. Computational complexity analysis of segmentation models on sentinel-2 dataset.

Landsat-8			
Model Variant	**Model Variant**	**Model Variant**	**Model Variant**
U-Net v5	31.2	43.9	115
Attention U-Net	34.5	46.7	130
U-Net++	38.1	50.9	145
DDMSA-U-Net v5	29.7	39.8	105

4.4 Ablation study

This section isolates the contributions of the DWSC, DC, and MSA components through systematic ablation. The results show that each component independently improves the segmentation metrics; however, their combined integration yields the highest performance gains. This allowed us to evaluate the significant contribution of each component, as shown in Figure 5.

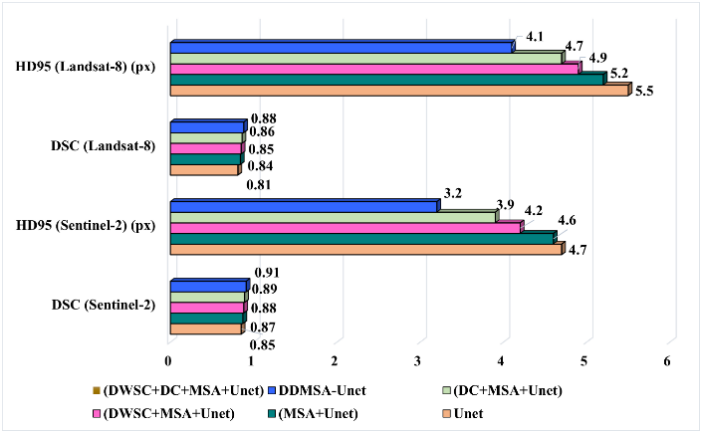

Fig. 5. Ablation study results showing the impact of architectural components (DWSC, DC, MSA) on segmentation performance across sentinel-2 and landsat-8.

4.5 Statistical analysis

Two-way ANOVA was performed to determine the statistical significance of the model's performance on different datasets and change classes. The results indicate that the type of dataset and change class have a significant impact on the correctness of segmentation ($p < 0.05$), with Sentinel-2 performing better in all the cases. The results demonstrate the flexibility of the model and mimic its soundness in varying farm situations, reiterating the effectiveness of its forecast in the Table 5.

Table 5. Two-way ANOVA results comparing classification accuracy between sentinel-2 and landsat-8 datasets across land-use change classes.

Metric	dataset F-value	dataset p-value	Change Class F-value	Change Class p-value	Interaction F-value	Interaction p-value
Producer's Accuracy	6.21	0.015	8.34	0.0008	2.12	0.07
User's Accuracy	5.89	0.019	7.76	0.0009	1.98	0.08
Kappa Coefficient	4.45	0.032	6.91	0.002	1.67	0.11

4.6 Discussion

The DDMSA-U-Net model performed well in the detection of seasonal shifts in land use using the Sentinel-2 and Landsat-8 sets. Its reliability was confirmed by consistently high overall accuracy greater than 91% and a kappa value is greater than 0.85. Upscaling transitions such as FallowLand to Wheat and Berseem to Built-up were identified with high precision and could be used to monitor crops. The architecture of the model, which is a combination of DWSCs, DCs, and the concept of multi-spatial attention, was successful in decreasing the computational overhead and, at the same time, increased the quality of segmentation. Nevertheless, there are still some limitations. The model requires cloud-free image data that may be classically inconsistent. There were specific change classes with missing or scarce data, which may have influenced the accuracy of detection. Moreover, depending on the type of crop or land-use pattern, regions/locales can exhibit different model performance. Nevertheless, these difficulties can be overcome in large-scale agricultural CD using DDMSA-U-Net, as demonstrated by the results. Future research must address soundness in the face of data gaps and cross-country testing.

5 Conclusion

In this research, a DL model of DDMSA-U-Net was suggested as the mechanism of land-use CD based on Landsat-8 and Sentinel-2 datasets. The model combines DWSCs, DMSFE, and spatial attention to enhance segmentation precision and minimize computation. When compared to standard U-Net variants, DDMSA-U-Net improved in terms of classification and CD with an overall accuracy of 91.6-96.6 and Kappa values above 0.85 for all cases. The primary outcome is a lightweight and scalable design that can perform well over datasets and seasons. It has been demonstrated to be adaptable, as it shows the same results across Sentinel-2 and Landsat-8 datasets. The changes include enhanced boundary detection and fewer false positives. The model can be used for real-time monitoring and can assist in agriculture and land management decision-making. Future work can apply quantization-aware training and pruning techniques to deploy DDMSA-U-Net on edge devices for real-time monitoring.

References

1. J. Chang, W. Du, B. Zhang, S. Guo, Y. Yin, Z. Wang, T. Xu, Z. Feng, Based on the improved EDCSTFN model, MODIS, Landsat 8 and Sentinel-2 data were fused to obtain 10 m dense time series images. IEEE Access **13**, 79189-79202 (2025). https://doi.org/10.1109/ACCESS.2025.3564968
2. I. Ituen, B. Hu, A multisource data approach for change and disturbance mapping of Ontario's Clay Belt towards more accurate carbon and emissions estimation. IEEE J. Sel. Top. Appl. Earth Obs. Remote Sens. **18**, 38-60 (2024). https://doi.org/10.1109/JSTARS.2024.3491804
3. W. Zhao, R. Lyu, J. Zhang, J. Pang, J. Zhang, A fast hybrid approach for continuous land cover change monitoring and semantic segmentation using satellite time series. Int. J. Appl. Earth Obs. Geoinf. **134**, 104222 (2024). https://doi.org/10.1016/j.jag.2024.104222
4. X. Zhong, Y. Du, X. Wang, X. Li, W. Zhao, Y. Zhang, P.M. Atkinson, Monitoring annual forest cover fraction change during 2000–2020 in China's Han River Basin using time-series MODIS NDVI, VCF and spatio-temporal regression. IEEE J. Sel. Top. Appl. Earth Obs. Remote Sens. **17**, 12092-12111 (2024). https://doi.org/10.1109/JSTARS.2024.3417302
5. A. Atesoglu, H.B. Ozel, T. Varol, M. Cetin, B.U. Baysal, F.S. Bulut, Monitoring land cover/use conversions in Türkiye wetlands using Collect Earth. J. Indian Soc. Remote Sens. **53**, 1979-1994 (2025). https://doi.org/10.1007/s12524-024-02111-w
6. L. Feng, S. Hussain, N.G. Pricope, S. Arshad, A. Tariq, L. Feng, M. Mubeen, R.W. Aslam, M.S. Fnais, W. Li, H. El-Askary, Seasonal dynamics in

land surface temperature in response to land use land cover changes using Google Earth Engine. IEEE J. Sel. Top. Appl. Earth Obs. Remote Sens. **17**, 17983-17997 (2024). https://doi.org/10.1109/JSTARS.2024.3466191

7. S.S. Wahla, J.H. Kazmi, A. Tariq, Mapping and monitoring of spatio-temporal land use and land cover changes and relationship with normalized satellite indices and driving factors. Geol. Ecol. Landscapes **9**, 279-295 (2025). https://doi.org/10.1080/24749508.2023.2187567
8. H. Li, Q. Miao, H. Shi, X. Li, S. Zhang, F. Zhang, H. Bu, P. Wang, L. Yang, Y. Wang, H. Du, Remote sensing monitoring of irrigated area in the non-growth season and of water consumption analysis in a large-scale irrigation district. Agric. Water Manage. **303**, 109020 (2024). https://doi.org/10.1016/j.agwat.2024.109020
9. M. Nyamtseren, T.D. Pham, T.T.P. Vu, I. Navaandorj, K. Shoyama, Mapping vegetation changes in Mongolian grasslands (1990–2024) using Landsat data and advanced machine learning algorithm. Remote Sens. **17**, 400 (2025). https://doi.org/10.3390/rs17030400
10. S. Yuan, Z. Mei, C. Zhu, R. Cao, S. Li, L. Yang, Y. Su, W. Li, Investigating the spatio-temporal interactive relationship between land use structure and ecosystem services in urbanizing China. Ecol. Indic. **158**, 111315 (2024). https://doi.org/10.1016/j.ecolind.2023.111315
11. R.O. Muchelo, T.F. Bishop, S.U. Ugbaje, S.I. Akpa, Patterns of urban sprawl and agricultural land loss in sub-Saharan Africa: the cases of the Ugandan cities of Kampala and Mbarara. Land **13**, 1056 (2024). https://doi.org/10.3390/land13071056
12. X. Wang, B. Chen, J. Dong, Y. Gao, G. Wang, H. Lai, Z. Wu, C. Yang, W. Kou, T. Yun, Early identification of immature rubber plantations using Landsat and Sentinel satellite images. Int. J. Appl. Earth Obs. Geoinf. **133**, 104097 (2024). https://doi.org/10.1016/j.jag.2024.104097
13. H. Zhang, K. Luo, A. Samat, C. Zhu, T. Jiao, ACO-TSSCD: an optimized deep multimodal temporal semantic segmentation change detection approach for monitoring agricultural land conversion. Agronomy **14**, 2909 (2024). https://doi.org/10.3390/agronomy14122909
14. M. Majnoun Hosseini, M.J. Valadan Zoej, A. Taheri Dehkordi, E. Ghaderpour, Cropping intensity mapping in Sentinel-2 and Landsat-8/9 remote sensing data using temporal transfer of a stacked ensemble machine learning model within Google Earth Engine. Geocarto Int. **39**, 2387786 (2024). https://doi.org/10.1080/10106049.2024.2387786
15. C. Eisfelder, B. Boemke, U. Gessner, P. Sogno, G. Alemu, R. Hailu, C. Mesmer, J. Huth, Cropland and crop type classification with Sentinel-1 and Sentinel-2 time series using Google Earth Engine for agricultural monitoring in Ethiopia. Remote Sens. **16**, 866 (2024). https://doi.org/10.3390/rs16050866
16. The landsat-8 dataset link: https://earth.esa.int/eogateway/missions/landsat-8 (accessed on 14/08/25)
17. The sentinel-2 dataset link: https://dataspace.copernicus.eu/explore-data/data-collections/sentinel-data/sentinel-2 (accessed on 14/08/25)